NANO LETTERS

2003
Vol. 3, No. 7
919−923

Electrochemical Growth of Single-Crystal Metal Nanowires via a Two-Dimensional Nucleation and Growth Mechanism

Mingliang Tian,*[,†,‡] Jinguo Wang,[†] James Kurtz,[†,‡] Thomas E. Mallouk,[†,§] and M. H. W. Chan[†,‡]

The Materials Research Institute, Pennsylvania State University, University Park, Pennsylvania 16802-6300, Department of Physics, 104 Davey Laboratory, Pennsylvania State University, University Park, Pennsylvania 16802-6300, and Department of Chemistry, 108 Davey Laboratory, Pennsylvania State University, University Park, Pennsylvania 16802-6300

Received April 10, 2003; Revised Manuscript Received May 28, 2003

ABSTRACT

Metallic nanowires (Au, Ag, Cu, Ni, Co, and Rh) with an average diameter of 40 nm and a length of 3–5 μm have been fabricated by electrodeposition in the pores of track-etched polycarbonate membranes. Structural characterizations by transmission electron microscopy (TEM) and electron diffraction showed that nanowires of Au, Ag, and Cu are single-crystalline with a preferred [111] orientation, whereas Ni, Co, and Rh wires are polycrystalline. Possible mechanisms responsible for nucleation and growth for single-crystal noble metals versus polycrystalline group VIII-B metals are discussed.

One-dimensional (1D) metallic nanowires have attracted considerable attention in recent years because of their novel physical properties and potential applications as interconnects in future generations of nanometer-scale electronics. There are a few methods for preparing nanowires of controlled length and diameter. One of the most successful approaches to fabricating large numbers of wires with high aspect ratios is electrochemical replication of the cylindrical pores of nonconductive porous membranes.[1−4] However, most 1D nanowires made by electrodeposition are polycrystalline in nature. Recently, several groups[5−7] reported the electrochemical growth of copper single-crystal wires in polycarbonate and anodic alumina membranes by a reverse pulse technique in ultrasonic fields or by conventional dc plating at room temperature. The diameters of these wires range from micrometers down to nanometers (∼70 nm). Similarly, Pb, Bi, and Ag single-crystalline wires[8−10] have also been fabricated by electrodeposition. It appears that if lower overpotential is used during deposition then single-crystalline nanowires of Cu, Ag, and other low melting point metals such as Pb and Bi can be grown, but the growth mechanism and the relationship between the overpotential and the crystalline structures of nanowires are not entirely clear. However, for high melting point metals such as Co, Ni, Rh, and Pt, single-crystal growth via electrodeposition is very difficult and has not been reported so far.

In this paper, we describe an effective method for preparing single-crystalline Au, Ag, and Cu nanowires by electrochemical deposition. The addition of Au to the list of single-crystalline wires is important because Au is widely used as a substrate for self-assembled monolayers (SAMs).[11,12] A number of SAM-based molecular electronic devices have recently been reported.[13−15] High-resolution transmission electron microscopy (HRTEM) and electron diffraction (ED) show that the crystalline structures of noble metals are sensitive to the electrodeposition parameters (overpotential, temperature, and additive). The texture of wires can be tuned from typical polycrystalline to bamboolike structures and then to single-crystalline structures by reducing the depositing potential. It is found that the single-crystal nanowires grow epitaxially, primarily along the [111] direction, by a two-dimensional (2D) nucleation/growth mechanism. For group

* Corresponding author. E-mail: mut1@psu.edu. Tel: (814) 863-5344. Fax: (814) 865-3604.
† The Materials Research Institute.
‡ Department of Physics.
§ Department of Chemistry.

10.1021/nl034217d CCC: $25.00 © 2003 American Chemical Society
Published on Web 06/20/2003

VIIIB metals (Co, Ni, and Rh), they always showed polycrystalline structures, and the textures are insensitive to the depositing parameters. TEM pictures showed that the polycrystalline growth of metallic nanowires appears to proceed in the typical three-dimensional (3D) nucleation−coalescence manner.

Electrodeposition was performed in a glass tube cell at about 40 °C. Platinum wire and a saturated calomel electrode (SCE) were used as the counterelectrode and reference electrode, respectively. The electrolytes for Au, Ag, Cu, Co, Ni, and Rh depositions were prepared as follows: (a) A small amount of gelatin (about 2 wt %) was added to a 20-mL commercial Orotemp Au or 1025 Ag bath (Technic Inc), which was then diluted with water to 40 mL for Au or Ag deposition. (b) A $CuSO_4 \cdot 5H_2O$ (0.5 M) with 1% gelatin (by weight) aqueous solution was used for Cu deposition, with the pH value adjusted to 1 with concentrated H_2SO_4. (c) Co (or Ni) solution contained 0.2 M $CoSO_4 \cdot xH_2O$ (0.1 M $NiSO_4 \cdot 6H_2O$), 0.1 M H_3BO_3 (0.7 M H_3BO_3) and 1% gelatin (by weight). (d) The Rh solution was prepared by dissolving 0.25 g of $RhCl_3$ in 20 mL of water; then 0.5 g of NaOH and 6 mL of concentrated H_2SO_4 were added before the solution was diluted to 125 mL with water. Commercial polycarbonate membranes (SPI Probe Inc.) with nominal pore sizes of 10 nm were used as templates. The thickness and pore density of the membranes are, respectively, 6 μm and 6×10^8 pores/cm^2. A thin Au film with a thickness of 200 nm evaporated on one side of the membrane served as the cathode lead. During the initial 1−2 min of the electrodeposition, a more negative potential was required to deposit metals into the pores. After the initial higher negative potential step, a steady lower deposition voltage, V_{SCE}, was maintained. Without the initial higher negative potential step, metal tends to grow laterally onto the conducting film instead of into the pores. The nanowires were harvested by dissolving the polycarbonate membrane in dichloromethane and precipitating from the solvent by means of a centrifuge. The free-standing nanowires were stored as a suspension in ethyl alcohol. TEM specimens were prepared by placing a drop of the nanowire suspension on a Lacey carbon grid.

Figure 1a shows a typical TEM image of free-standing Au nanowires made at a potential of $V_{SCE} = -0.75$ V. The average diameter of the wires is 40 nm, which is 4 times larger than the nominal pore size of 10 nm reported by the manufacturer of the porous membranes. This is consistent with the findings of Schonenberger et al.[16] The porous membranes are usually used for filtration purposes, and it appears that the nominal pore diameters quoted by the manufacturer are the values of the pore opening near the surface. We found that the diameter of each wire is narrower on both ends of the wire, as seen in Figure 4a−c. Figure 1b shows a TEM image of a segment of a randomly selected Au nanowire and the corresponding electron diffraction (ED) pattern. The ED pattern of the Au nanowire does not change along the length of the wire, but the intensity of the individual spots show a slight variation. This means that the nanowire is a single crystal with a slight structural deformation along its length. The ED pattern showed that the growth orientation

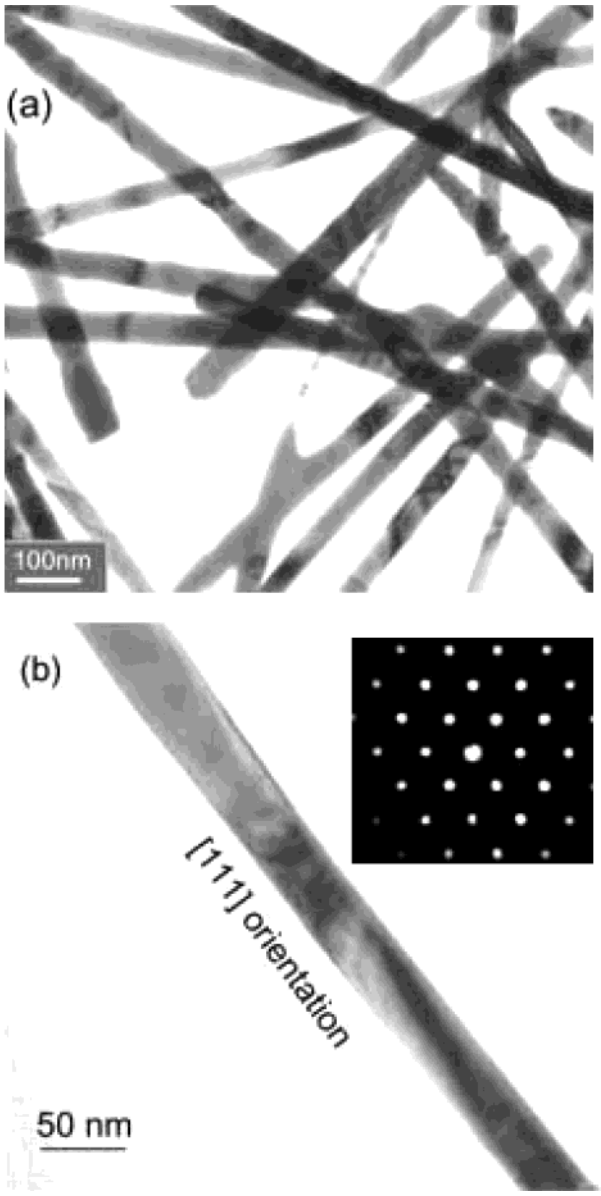

Figure 1. (a) TEM image of free-standing Au nanowires. (b) TEM image of a randomly selected Au wire showing the [111] growth direction and the electron diffraction pattern.

of this wire is along the [111] direction. We randomly checked several tens of these nanowires; 90% of them showed [111] orientation, and fewer than 10% showed [100], [110], and [11$\bar{2}$] orientations. This was further confirmed by X-ray diffraction experiments performed on an array of nanowires still embedded in the membrane.

Figure 2 shows a HRTEM image of the growth tip of a thin Au nanowire; the diameter of the tip is about 14 nm. Inset a shows the ED pattern of the tip, and insets b and c show, respectively, the locally enlarged HRTEM image and the ED pattern of the marked area. The nanowire shows single-crystal texture for the [111] orientation. The (200), (111), and (1$\bar{1}\bar{1}$) atomic surfaces are imaged on the tip. A twin boundary across the wire is seen clearly, and the twinning elements are given in inset b. The twin system is (111)[11$\bar{2}$], which is the primary twinning system in fcc noble metals.

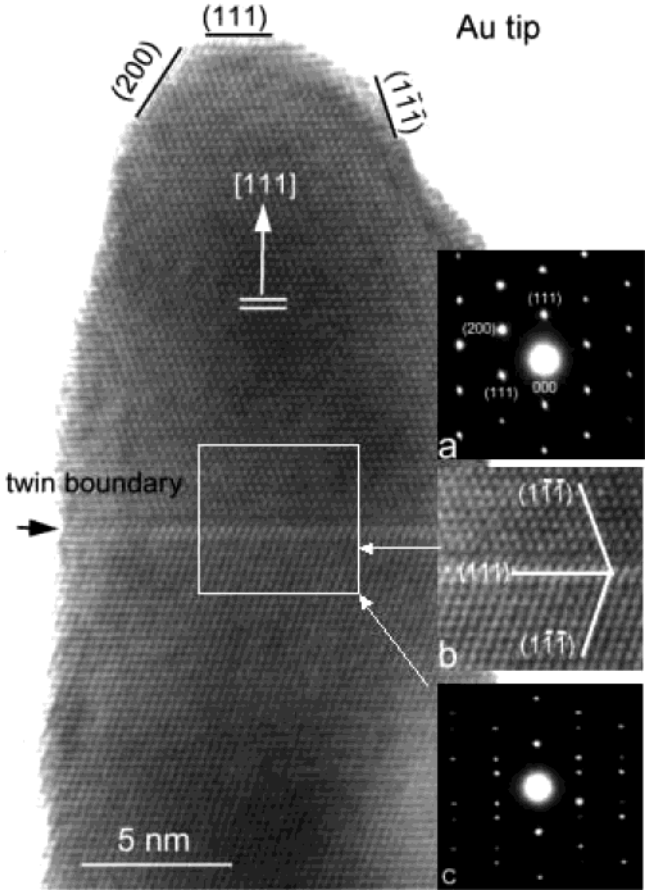

Figure 2. HRTEM image of an Au wire tip showing the [111] growth direction. (200), (111), and (1$\bar{1}\bar{1}$) atom surfaces and a twin boundary transverse to the wire axis are indicated. Inset a is the electron diffraction pattern of the tip. Insets b and c are, respectively, a locally enlarged HRTEM image and the electron diffraction pattern of the twin boundary area.

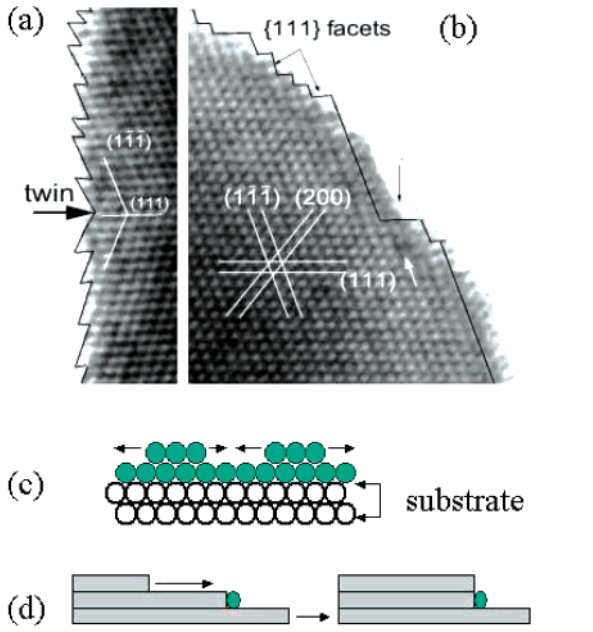

Figure 3. (a) Magnified HRTEM images of part of the lateral surface and of the top surface of the Au tip shown in Figure 2. The solid lines show profiles of atomic-height steps with {111} facets. (b) and (c) show schematic representations of the layer growth model and the bunching steps, respectively.

The most interesting feature in this image is that the rows of surface atoms are imaged clearly so that we can delineate the growth mechanism of the nanowires. Figure 3a and b show, respectively, locally enlarged portions of HRTEM images of the lateral and tip surfaces. The surface structures are clearly resolved on the atomic scale. Monatomic and multiatomic steps are indicated by thin solid lines. From these images, it is apparent that the surfaces of the Au nanorods are facetted on the atomic scale and that there is no surface reconstruction. These atomic-height microsteps are formed by {111} facets. This is consistent with similar observations made with gold nanodot crystals.[17,18] Because the {111} surface is the most densely packed and hence the energetically most favorable surface for fcc Au, the formation of {111} facets on the Au rod surface is expected. In a recent experiment in which gold nanorods were capped with micelles,[19] in addition to {100} facets (another low-energy surface), {110} facets with surface reconstruction were also observed. These {110} facets are not observed in our free-standing Au nanowires, but {100} surfaces are seen on the tip. It is possible that micelles can stabilize the normally energetically unfavorable {110} facets. The observation of {111} facets with single and multiatomic height steps on the wire surface is direct evidence of a 2D layer growth mechanism. A schematic representation of 2D layer growth and the bunching process of atomic steps is illustrated in Figure 3c and d, respectively.

Single-crystal Ag and Cu nanowires were also fabricated using similar electrodeposition conditions with depositing potentials smaller than −0.9 and −0.015 V, respectively. TEM images showed that Ag and Cu nanowires also grow mainly along the [111] direction. {111}-facetted atomic-height steps are also observed on the surface of Ag nanowires. The morphology of the Au, Ag, and Cu nanowires strongly depends on the deposition parameters. It appears that three factors—the gelatin additive, elevated temperature, and low overpotential—used in the deposition are crucial to the growth of single-crystalline Au, Ag, and Cu nanowires. When one or more of these conditions are not met, bamboolike or completely polycrystalline nanowires are found. To study the dependence of the morphology of the nanowire as a function of the overpotential, we carried out deposition on three different membranes at a fixed temperature of 40 °C using the same gelatin-modulated solution with a slightly different protocol in varying potentials. Each deposition was carried out in the following manner: a higher overpotential (−1.1, −1.2, or −1.0 V) was applied in the first 1 or 2 min and then reduced to a lower value (−0.7, −0.9, or 0.85 V) for about 10 min. The TEM images of these Au nanowires are shown in Figure 4a−c, respectively. The insets of Figure 4a and c, respectively, show the locally enlarged TEM images indicated by the box. It is seen that the tips of the nanowires made at a more negative overpotential, −1.2, −1.1, or −1.0 V, showed typical polycrystalline structures, and the average grain size increases

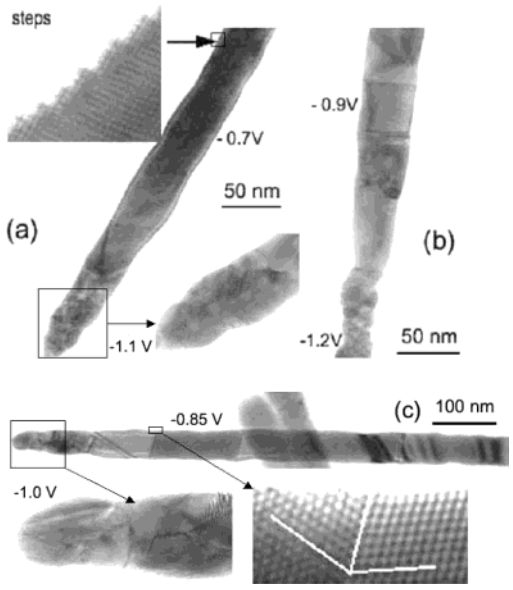

Figure 4. TEM images of Au nanowires deposited with varying potentials. (a) −1.1, −0.7 V; (b) −1.2, −0.9 V; (c) −1.0, −0.85 V. The insets, respectively, show the locally enlarged TEM images of the areas indicated by the boxes.

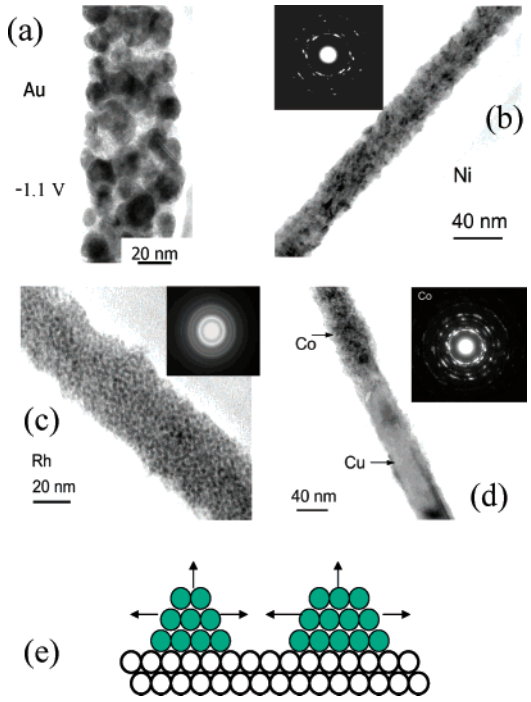

Figure 5. (a−c) TEM images of polycrystalline Au, Ni, and Rh nanowires deposited at V_{SCE} = −1.1, −1.1, and −0.25 V, respectively. (d) Junction of a Co/Cu striped nanowire and the ED pattern of a Co wire; single-crystalline Cu and polycrystalline Co were deposited at −0.015 and −1.1 V, respectively. (e) Schematic representation of the 3D nucleation−coalescence growth model.

when the potential is reduced. The spherical shape of grains formed at −1.2 V reflects a typical 3D nucleation process during the deposition. When the value of the potential is reduced below about −1.0 V, bamboolike crystalline structure resulted, and the length of the single-crystalline segment increases when the potential is reduced, as shown in Figure 4b and c. Most of the boundaries between the two single-crystal segments are (111)[11$\bar{2}$] twin boundaries, as seen in the inset of Figure 4c. When the potential is reduced below −0.75 V, completely single-crystalline growth occurred, as seen in Figure 4a. Monatomic and multiatomic steps were clearly seen on the surface of the single-crystalline segments of the wires, as shown in the inset of Figure 4a and c. This Figure also shows that single-crystalline Au nanowires can be grown directly from polycrystalline seeds by adjusting the depositing potential, but the intervening segment between the polycrystal and single-crystal regime contains more defects. Figure 5a shows a typical polycrystalline Au nanowire obtained using the commercial Au bath without gelatin, at 17 °C and at a potential of −1.1 V. The size of the spherical grains is about 12−18 nm, which is comparable to the size of those shown in Figure 4b, but the wire of Figure 5a showed many voids between the grains. This indicates that a number of 3D nuclei grew simultaneously and independently of each other.

TEM images of Ni and Rh nanowires and their ED patterns are shown in Figure 5b and c, respectively. The junction region of a Co/Cu striped nanowire and the ED pattern of a Co wire are also shown in Figure 4d. The Co, Ni, and Rh wires were invariably polycrystalline, and their grain sizes were about 2−5 nm for Rh and 2−8 nm for Ni and Co. The grain size is much smaller than that of the polycrystalline Au nanowires shown in Figure 4 and Figure 5a. The grain boundaries of these group VIIIB nanowires are irregular with a great deal of void space. This indicates that, for Co, Ni, and Rh nanowires, the growth follows a typical 3D nucleation−coalescence mechanism.[20] A schematic representation of 3D nucleation−coalescence growth is given in Figure 5e. In contrast to Au and the other soft metals studied, the texture of the Co, Ni, and Rh wires is relatively insensitive to the overpotential and the temperature maintained during the electrodeposition. The addition of gelatin also had no clear effect on the morphology of these wires. It appears that the above-mentioned dc plating method is not suitable for the single-crystal growth of these high melting point group VIIIB metals, but we cannot exclude the possibility of single-crystal growth using other techniques under pulse or ultrasonic conditions.

The reasons that lower overpotential, elevated temperature, and a gelatin additive favor the single-crystal growth of noble metal nanowires but not higher melting point group VIIIB wires are not entirely clear. It is interesting that the polycrystalline noble metal nanowires show much larger grain sizes than the group VIIIB wires. During electrochemical deposition, new grains will grow if the size of an initial cluster exceeds the critical dimension N_c.[20] The larger the N_c is, the more favorable it is for a single crystal to grow from a previously nucleated seed grain. The critical dimension N_c for a 2D-like nucleus can be expressed as $N_c = bs\epsilon^2/(Ze\eta)^2$, where s, ϵ, Z, η, and b are the area occupied by one atom on the surface of the nucleus, the edge energy, the effective electron number, the overpotential, and a constant, respectively.[20] During electrodeposition, the only parameter that we can change is the overpotential η. If η is low, then

single-crystal growth is favored because N_c is large. Our results shown in Figure 4 are in agreement with this scenario. The elevated temperature promotes the surface diffusions of atoms and favors the growth of preexisting nuclei established during the first 1−2 min at a higher overpotential. At lower temperatures and high potential, the 3D nuclei tend to grow simultaneously and independently of each other, as seen in Figure 5a. The effect of the gelatin additive is not as easily explained. It is possible that the gelatin additive promotes the wetting of the pores of the membrane by the electrolyte; thus, the surface energy involved in depositing metallic ions into nanopores is reduced, and deposition can occur at a lower overpotential.

Relative to noble metals, group VIIIB metals have smaller atomic volumes and higher effective electron numbers, Z, resulting in a smaller critical dimension N_c for 2D nucleation. Co, Ni, and Rh have much higher melting points ($T_m \approx$ 2700−3700 °C) and higher binding energies and thus favor the aggregation of atoms into small 3D clusters. The diffusion of electrodeposited atoms along the surface is inhibited by the high cohesive energy of these metals, resulting in the nucleation, growth, and coalescence of many 3D grains during deposition. Therefore, single-crystal growth via a 2D layer-by-layer epitaxial mechanism is relatively facile for low melting point metals such as Pb, Sn, and Bi ($T_m \approx$ 200−320 °C) at room temperature and for noble metals Ag, Au, and Cu ($T_m \approx$ 960−1100 °C) at slightly elevated temperatures.

Acknowledgment. We acknowledge useful discussions with Achim Amma, Brian Kelley, Sarah St. Angelo, Mahy El-Kouedi, and Christine Keating. This work was supported by National Science Foundation (NSF) grants DMR 0080019 and DMR 0213623.

References

(1) (a) Foss, C. A.; Tierney, M. J.; Martin, C. R. *J. Phys. Chem.* **1992**, *96*, 9001. (b) Martin C. R. *Chem. Mater.* **1996**, *8*, 1739. (c) Sapp, S. A.; Mitchell, D. T.; Martin, C. R. *Chem. Mater.* **1999**, *11*, 1183. (d) Martin, C. R. *Science* **1994**, *266*, 1961. (e) Hulteen, J. C.; Martin, C. R. *J. Mater. Chem.* **1997**, *7*, 1075. (f) Martin, B. R.; Dermody, D. J.; Reiss, B. D.; Fang, M.; Lyon, L. A.; Natan, M. J.; Mallouk, T. E. *Adv. Mater.* **1999**, *11*, 1021.
(2) (a) Preston, C. K.; Moskovits, M. *J. Phys. Chem.* **1993**, *97*, 8495. (b) Routkevitch, D.; Bigioni, T.; Moskovits, M.; Xu, J. M. *J. Phys. Chem.* **1996**, *100*, 14037.
(3) (a) Whitney, T. M.; Jiang, J. S.; Searson, P. C.; Chien, C. L. *Science* **1993**, *261*, 1316. (b) Sun, L.; Searson, P. C.; Chien, C. L. *Phys. Rev. B* **2000**, *61*, R6463. (c) Liu, K. L.; Chien, C. L.; Searson, P. C.; Zhang, K. Y. *Appl. Phys. Lett.* **1998**, *73*, 1436.
(4) Zeng, H.; Zheng, M.; Skomski, R.; Sellmyer, D. J.; Liu, Y.; Menon, L.; Bandyyopadhyay, S. *J. Appl. Phys.* **2000**, *87*, 4718.
(5) Dobrev, D.; Vetter, J.; Angert, N.; Neumann, R. *Appl. Phys. A* **1999**, *69*, 233.
(6) Molares, M. E. T.; Buschmann, V.; Dobrev, D.; Neumann, R.; Scholz, R.; Schuchert, I. U.; Vetter, J. *Adv. Mater.* **2001**, *13*, 62.
(7) Gao, T.; Meng, G. W.; Wang, Y. W.; Sun, S. H.; Zhang, L. D. *J. Phys.: Condens. Matter* **2002**, *14*, 355.
(8) Yi, G.; Schwarzacher, W. *Appl. Phys. Lett.* **1999**, *74*, 1746.
(9) Wang, X. F.; Zhang, J.; Shi, H. Z.; Mang, Y. W.; Meng, G. W.; Peng, X. S.; Zhang, L. D.; Fang, J. *J. Appl. Phys.* **2001**, *89*, 3847.
(10) Zhang, J.; Wang, X.; Peng, X.; Zhang, L. *Appl. Phys. A* **2002**, *75*, 485.
(11) Chen, J.; Reed, M. A.; Rawlett, A. M.; Tour, J. M. *Science* **1999**, *286*, 1550.
(12) Reed, M. A.; Chen, J.; Rawlett, A. M.; Price, D. W.; Tour, J. M. *Appl. Phys. Lett.* **2001**, *78*, 3735.
(13) Kwok, K. S.; Ellenbogen, J. C. *Mater. Today* **2002**, *5*, 28.
(14) Tseng, G. Y.; Ellenbogen, J. C. *Science* **2001**, *294*, 1293.
(15) Joachim, C.; Gimzewski, J. K.; Aviram, A. *Nature* **2000**, *408*, 541.
(16) Schonenberger, C.; van der Zande, B. M. I.; Fokkink, L. G. J.; Henny, M.; Schmid, C.; Kruger, M.; Bachtol, A.; Huber, R.; Birk, H.; Staufer, U. *J. Phys. Chem. B* **1997**, *101*, 5497.
(17) Flueli, M.; Spycher, R.; Stadelmann, P. A.; Buffat, P. A.; Borel, J. P. *Europhys. Lett.* **1988**, *6*, 349.
(18) Marks, L. D. *Rep. Prog. Phys.* **1994**, *57*, 603.
(19) Wang, Z. L.; Mohamed, M. B.; Link, S.; El-Sayed, M. A. *J. Phys. Chem. B* **1998**, *103*, 11.
(20) Paunovic, M.; Schlesinger, M. *Fundamentals of Electrochemical Deposition*; Wiley: New York, 1998; pp 108−109.

NL034217D